A mutation leading to super-assembly of twin-arginine translocase (Tat) protein complexes

Patel, Roshani; Vasilev, Cvetelin; Beck, Daniel; Monteferrante, Carmine G; van Dijl, Jan Maarten; Hunter, C Neil; Smith, Corinne; Robinson, Colin

Published in:
Biochimica et Biophysica Acta - Molecular Cell Research

DOI:
10.1016/j.bbamcr.2014.05.009

Publication date:
2014

Biochimica et Biophysica Acta 1843 (2014) 1978–1986

Contents lists available at ScienceDirect

Biochimica et Biophysica Acta

journal homepage: www.elsevier.com/locate/bbamcr

A mutation leading to super-assembly of twin-arginine translocase (Tat) protein complexes

Roshani Patel [a], Cvetelin Vasilev [b], Daniel Beck [a], Carmine G. Monteferrante [c], Jan Maarten van Dijl [c], C. Neil Hunter [b], Corinne Smith [a], Colin Robinson [d,*]

[a] School of Life Sciences, Gibbet Hill Campus, The University of Warwick, Coventry CV4 7AL, UK
[b] Department of Molecular Biology and Biotechnology, University of Sheffield, Sheffield S10 2TN, UK
[c] Department of Medical Microbiology, University of Groningen, University Medical Center Groningen, Groningen, The Netherlands
[d] Centre for Molecular Processing, School of Biosciences, University of Kent, Canterbury CT2 7NJ, UK

ARTICLE INFO

Article history:
Received 14 February 2014
Received in revised form 16 May 2014
Accepted 19 May 2014
Available online 26 May 2014

Keywords:
Tat
Twin-arginine translocation
Signal peptide
Atomic force microscopy
AFM

ABSTRACT

The Tat system transports folded proteins across the bacterial plasma membrane. The mechanism is believed to involve coalescence of a TatC-containing unit with a separate TatA complex, but the full translocation complex has never been visualised and the assembly process is poorly defined. We report the analysis of the *Bacillus subtilis* TatAyCy system, which occurs as separate TatAyCy and TatAy complexes at steady state, using single-particle electron microscopy (EM) and advanced atomic force microscopy (AFM) approaches. We show that a P2A mutation in the TatAy subunit leads to apparent super-assembly of Tat complexes. Purification of TatCy-containing complexes leads to a large increase in the TatA:TatC ratio, suggesting that TatAy^{P2A} complexes may have attached to the TatAyCy complex. EM and AFM analyses show that the wild-type TatAyCy complex purifies as roughly spherical complexes of 9–16 nm diameter, whereas the P2A mutation leads to accumulation of large (up to 500 nm long) fibrils that are chains of numerous complexes. Time lapsed AFM imaging, recorded on fibrils under liquid, shows that they adopt a variety of tightly curved conformations, with radii of curvature of 10–12 nm comparable to the size of single TatAy^{P2A} complexes. The combined data indicate that the mutation leads to super-assembly of TatAy^{P2A} complexes and we propose that an individual TatAy^{P2A} complex assembles initially with a TatAy^{P2A}Cy complex, after which further TatAy^{P2A} complexes attach to each other. The data further suggest that the N-terminal extracytoplasmic domain of TatAy plays an essential role in Tat complex interactions.

1. Introduction

The Tat system transports folded proteins across the plasma membrane in a wide range of bacteria, using a mechanism that remains poorly understood [1–3]. In Gram-negative bacteria, the core components of the system are membrane-bound TatABC subunits which form distinct TatABC and TatA complexes at steady state. The TatABC complex binds substrates bearing N-terminal twin-arginine signal peptides, after which a separate TatA complex is recruited to form the full translocation system [3–6]. The TatA and TatB subunits share significant similarity but carry out distinct functions: the TatB subunit is only found complexed to TatC in the TatABC complex, whereas the TatA subunit is mostly present as a separate homo-oligomeric complex, with a small proportion associated with the TatBC subunits [6]. The fully-active translocon containing both sub-complexes has not been isolated or studied in great detail, however, and many aspects of the overall translocation mechanism remain poorly defined.

Gram-positive bacteria almost always contain a simpler, 'minimal' Tat system comprising only TatAC subunits [2,7–9]. *Bacillus subtilis* contains two such systems, termed TatAdCd and TatAyCy, that act in parallel. Studies on these systems have shown that the TatA-type subunits (TatAd and TatAy) are bifunctional, carrying out both TatA- and TatB-type functions as defined in Gram-negative bacteria [8–10]. As with the well-studied *Escherichia coli* system, two distinct Tat complexes are present at steady state: a TatAC complex and a separate TatA complex [8,11]. It appears likely that these are analogous to the *E. coli* TatABC and TatA complexes, respectively, but this issue has yet to be resolved.

Structural studies on Tat complexes have been carried out in an attempt to understand the unusual translocation mechanism which enables a wide variety of fully folded proteins to be transported. Initial studies on the *E. coli* system showed that the TatA complex is highly heterogeneous, ranging from approximately 50 kDa to over 500 kDa in size [12]. Moreover, the complexes appeared to contain cavities that could potentially form translocation pores of varying diameter – a

* Corresponding author at: Centre for Molecular Processing, School of Biosciences, University of Kent, Canterbury CT2 7NJ, UK. Tel.: +44 1227 823443.
E-mail address: c.robinson-504@kent.ac.uk (C. Robinson).

http://dx.doi.org/10.1016/j.bbamcr.2014.05.009
0167-4889/

possible means of transporting proteins of varying dimensions. However, *E. coli* also contains a TatA paralogue, TatE, which is capable of substituting for TatA when overexpressed, and studies on this complex showed it to be much smaller and more homogeneous [13]. Subsequent electron microscopy studies on TatA complexes from *B. subtilis* pointed to a similar situation: the TatAd and TatAc complexes were found to be small, homogeneous and only small potential pores were shown to be present [14]. These findings argue against a model in which translocation is mediated primarily by a single TatA-type complex of variable diameter, and suggest instead that other possibilities should be considered.

The 'Tat complex coalescence' issue is made more complicated by the fact that the active complexes have never been properly visualised. The current models rely heavily on crosslinking studies in which the substrate protein has been found crosslinked initially to TatBC and subsequently to TatA [15–18]. However, the lack of structural information on the assembled complexes has prevented exploration of the overall assembly process. In this report we have analysed Tat complexes containing a variant of the *B. subtilis* TatAy protein containing a single amino acid substitution. As explained above, TatAy is normally found in two relatively small, homogeneous complexes: TatAyCy (the presumed substrate-binding complex, analogous to the *E. coli* TatBC complex) and homo-oligomeric TatAy complexes [8,19,20]. Here we show that a P2A mutation in the extracytoplasmic region causes TatAy-containing complexes to apparently 'super-assemble' and form large fibrils. The data provide direct evidence for inter-complex assembly and point to a critical role of the short N-terminal section of this protein in mediating both TatAy–TatAyCy and TatAy–TatAy complex interactions.

2. Materials and methods

2.1. Strains and cultivation

B. subtilis strains were grown with agitation at 37 °C in either Lysogeny Broth (LB) medium or Paris minimal (PM) medium. LB medium consisted of 1% tryptone, 0.5% yeast extract and 1% NaCl, pH 7.4. PM consisted of 10.7 mg ml^{-1} K2HPO4, 6 mg ml^{-1} KHPO, 1 mg ml^{-1} trisodium citrate, 0.02 mg ml^{-1} MgSO4, 1% glucose, 0.1% casamino acids (Difco), 20 mg ml^{-1} L-tryptophan, 2.2 mg ml^{-1} ferric ammonium citrate and 20 mM potassium glutamate. *Lactococcus lactis* was grown at 30 °C in M17 broth supplemented with 0.5% (w/v) glucose and erythromycin 2 μg ml^{-1}. When required, media for *B. subtilis* were supplemented with erythromycin (2 μg ml^{-1}) or kanamycin (Km; 20 μg ml^{-1}).

2.2. Plasmid construction

To construct pNZ_AyCyP2A-His, which contains a mutated version of the *tatAy* gene, a copy of the *tatAy tatCy* operon was PCR amplified from the plasmid pHB-SDM-A2 [20] with a forward primer containing a *Bsp*HI restriction site and a reverse primer with a *Hin*dIII restriction site. The fragment was digested with *Bsp*HI–*Hin*dIII and cloned into *Nco*I–*Hin*dIII-digested pNZ8910. The ligation mixture was used to transform *L. lactis*, resulting in plasmid pNZ_AyCyP2A-His. This plasmid was then introduced into *B. subtilis* 168. To obtain the pNZ_AyCywt-His a mutagenesis was carried out using the F_Mut_tatAy and R_Mut_tatAy primers and the pNZ_AyCyP2A-His plasmid as a template.

Primers	
F_tatAyP2A	GGGGCCATGGCGATCGGTCCTG
R_tatAyP2Ahis	GGGGAAGCTTTTAGTGATGGTGATGGTGATGTTGCCCAGAAGACACGTC
F_Mut_tatAy	GTGACCACCATGCCGATCGGTCCTG
R_Mut_tatAy	CTCCTTTCAATACCTAAATAGTAACAGACAAATATCAAGATTTTATC

2.3. Expression of TatAyCy

B. subtilis 168 strains containing pNZ_AyCyP2A-His or pNZ_AyCywt-His were grown in LB medium at 37 °C under selective conditions (2 μg ml^{-1} erythromycin, 10 μg ml^{-1} kanamycin) until 0.6 OD_{600}. The expression of P2A TatAyCy or WT TatAyCy was then induced by addition of subtilisin-containing supernatant from *B. subtilis* ATCC 6633 [21]. After 3 h of induction, cells were harvested (4 °C, 3500 ×*g* for 20 min) and separated from the growth medium by centrifugation. Next, the cells were fractionated as described by Zweers et al. [22]. Briefly, the cells were incubated with lysozyme in protoplast buffer to liberate cell wall-associated proteins. The resulting protoplasts were collected by centrifugation and disrupted by bead-beating. Debris of the disrupted protoplasts was removed through centrifugation. Membranes were then separated from the cytoplasm through ultracentrifugation. Finally, the collected membranes were resuspended in solubilisation buffer with 0.1% DDM and left rotating overnight.

2.4. Purification of TatAyCy

10 ml of Talon resin was equilibrated with one column volume of buffer 1 (20 mM Tris–HCl pH 8.0, 400 mM NaCl, 5 mM imidazole and 0.02% DDM) and left rotating overnight at 4 °C. The resin was pelleted by centrifugation at 2000 rpm for 5 min to remove the buffer. The solubilised membranes were mixed with the equilibrated talon resin and left rotating for a minimum of 4 h at 4 °C. The slurry was then applied to a column and allowed to settle before collecting the flow-through. The column was washed with 6 column volumes of buffer 1 and then eluted with 2.5 column volumes of buffer 2 (20 mM Tris–HCl pH 8.0, 400 mM NaCl, 150 mM imidazole and 0.02% DDM). The elution fractions were collected in small aliquots, which were then analysed by SDS-PAGE and Western blotting with specific mouse anti-His IgG and horseradish peroxidase (HRP) conjugated anti-Mouse IgG. Bound antibodies were visualised using a chemiluminescence EZ-ECL detection kit. Peak fractions containing TatAyCy were concentrated using 10 kDa VivaSpin concentrators. For gel filtration analysis, the protein sample was centrifuged at 10,000 rpm for 10 min before injecting 0.24 ml onto a Superdex200 HR 10/30 column. The gel filtration run was carried out using buffer A (20 mM Trizma, 150 mM NaCl and 0.02% DDM). Eluted fractions were collected and TatAyCy complexes were detected by SDS-PAGE and Western blotting as indicated above.

2.5. Transmission electron microscopy

For transmission electron microscopy (TEM) of WT TatAyCy and P2A TatAyCy complexes, the peak elution fractions from the gel filtration chromatography were diluted to a concentration of ~10 ug/ml in buffer A before fixing to a grid. The grids were prepared as previously described [14]. Briefly, a carbon-coated grid (200 mesh, Agar scientific) was negatively glow-discharged for 1 min. Immediately, 4 ul of protein sample was applied for 1 min and washed twice with buffer A minus detergent. The grid was then stained twice for 20 s using 2% uranyl acetate and then air-dried for a minimum of 5 min. The grid was imaged under a 200 kV JEOL 2010 field emission gun (FEG) TEM with a 4 k Gatan Ultrascan CCD camera. Images were recorded at 40,000× magnification.

2.6. Atomic force microscopy sample preparation

For atomic force microscopy (AFM), the purified WT TatAyCy and $TatAy^{P2A}Cy$ complexes were diluted 10- or 50-fold in imaging buffer containing 10 mM Tris pH 7.4, 120 mM KCl, and 0.03% β-DDM. 40 μl of the protein solution was then deposited onto a freshly cleaved mica surface, created by stripping the top layer of a piece of mica, attached to a magnetic puck, using adhesive tape. The mica revealed by this process provides an atomically flat, hydrophilic substrate for subsequent

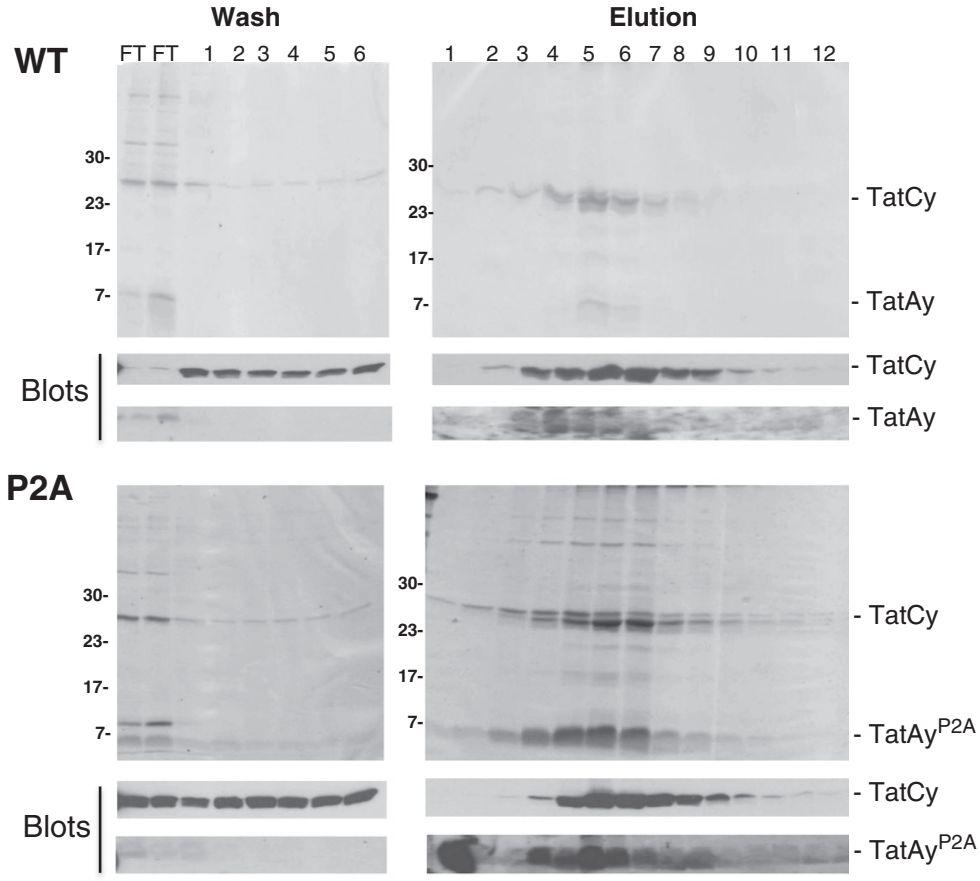

Fig. 1. The TatAy P2A mutation results in abnormal levels of TatAy in the purified TatAyCy complex. Wild-type TatAyCy proteins (WT) and the same proteins with a P2A mutation in TatAy (P2A) were expressed in *B. subtilis*. The membranes were then isolated and solubilised as detailed in the Materials and methods section, and the solubilised extract was applied to a Talon affinity column. The left hand panels show samples of the initial flow-through and wash fractions (FT, Wash); the right hand panels show the elution fractions. Upper panels show Coomassie-stained gels of the total protein, with the TatAy and TatCy protein bands indicated; the lower panels show immunoblots to detect TatCy and TatAy separately as indicated. The mobilities of molecular mass markers (in kDa) are indicated on the left.

AFM. After leaving the protein to adsorb for approximately 15 min, the sample was rinsed with an imaging buffer (3 times) and imaged with the AFM.

2.7. AFM measurements

The AFM data was collected in PeakForce QNM (PF-QNM) mode using a Multimode 8 instrument equipped with a 15 μm scanner (E-scanner) and coupled to a NanoScope Vcontroller (Bruker). NanoScope software (v8.15, Bruker) was used for data collection and Gwyddion (v2.31, open source software covered by GNU general public license, www.gwyddion.net) and OriginPro (v8.5.1,OriginLab Corp.) software was used for data processing and analysis. All measurements were performed at nearly-physiological conditions in buffer (10 mM Tris pH 7.4, 120 mM KCl, 0.03% β-DDM) at room temperature using BL-AC40TS probes (Olympus). The Z-modulation amplitude was adjusted to values in the range 20–24 nm, while the Z-modulation frequency was 2 kHz and the contact tip-sample force was kept in the range 60–80 pN.

3. Results

3.1. A P2A mutation in TatAy leads to hyper-accumulation of TatAy with TatCy

B. subtilis contains separate TatAdCd and TatAyCy systems, and previous studies have analysed the key regions in the TatAd and TatAy proteins using site-specific mutagenesis [8,10,19,20,23]. Both for TatAd and TatAy, it was shown that several of the extreme N-terminal residues are critical for translocation activity, and this is interesting because these are part of a very short N-terminal extracytoplasmic region; the vast majority of both TatAd and TatAy residues (indeed, of all TatA-family proteins) are located in the transmembrane span or cytoplasmic regions [8,20].

While these studies effectively delineated TatA- and TatB-type domains in these proteins, the effects of the mutations on Tat complex formation were not analysed in detail. In the present study we have used advanced imaging approaches to understand the effects of substituting Pro2 by Ala in the TatAy protein, which completely blocks TatAyCy translocation activity [20]. The TatAy^{P2A}Cy complex was overexpressed in *B. subtilis* and the non-mutated complex was analysed in parallel for control purposes. To monitor the effects on complex formation, both the wild-type and mutant *tatAyCy* operons were engineered such that a His-tag is attached to the C-terminus of TatCy, allowing direct purification of TatCy together with any TatAy that is bound to it. This procedure is therefore designed to isolate the TatAyCy complex since the untagged homo-oligomeric TatAy passes through the affinity column. For simplicity, the His-tagged, but otherwise wild-type TatAyCy complexes are still referred to as 'wild-type', or 'WT' hereafter. Our previous studies have shown that C-terminally tagged TatCy-containing complexes are active, although minor effects on activity or stability cannot be ruled out [11,20].

After expression in *B. subtilis*, the membrane fraction was isolated from cells expressing the WT or TatAy^{P2A}Cy complexes, solubilised in DDM and subjected to Talon chromatography to affinity-purify the His-tagged TatCy-containing complexes. Fig. 1 shows wash fractions

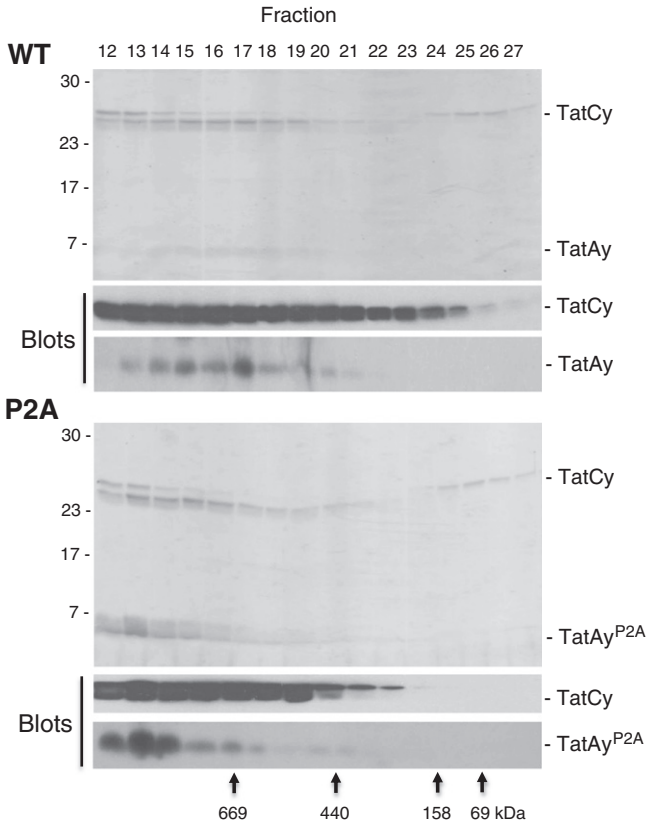

Fig. 2. Gel filtration of wild-type TatAyCy (WT) and TatAy^{P2A}Cy complexes (P2A). After concentration of the peak Talon elution fractions (shown in Fig. 1) the concentrated TatAyCy or TatAy^{P2A}Cy preparations were applied to a Superdex 200 gel filtration column. Upper panels show Coomassie-stained gels of the total protein, with the TatAy and TatCy bands indicated; the lower panels show immunoblots to detect TatCy and TatAy separately. The mobilities of SDS gel molecular mass markers (in kDa) are indicated on the left; peak elution fractions of marker proteins for the gel filtration column (in kDa) are indicated at the bottom of the figure.

and elution fractions obtained after elution of bound material. The upper panels represent the elution of WT TatAyCy complexes and the data clearly show that the tagged TatCy (25 kDa) is mostly present in the elution fractions as expected. The immunoblots show that the TatCy co-elutes with TatAy, confirming the presence of TatAyCy complexes. Furthermore, the Coomassie-stained gel shows that the complexes are relatively pure, with the TatCy band prominent and the TatAy band also clearly detectable.

TatAy^{P2A}Cy complexes containing the P2A mutation in TatAy were analysed in the same manner, and the lower panels of Fig. 1 show that TatCy is again purified to a significant extent during Talon affinity chromatography. The major difference is the presence of much greater levels of TatAy in the elution fractions. This is evident in the immunoblot, where the TatAy signal is much stronger than that in the WT elution profile, and also in the Coomassie-stained gel, where the TatAy band is now by far the most prominent band. These data provide initial evidence that the mutation leads to the assembly of abnormally high levels of TatAy with TatCy.

3.2. TatAy^{P2A}Cy complexes are larger than WT TatAyCy complexes

To investigate the effects of the P2A mutation on the size of the TatAyCy complexes, the peak elution fractions from the Talon affinity column were concentrated and applied to a Superdex 200 gel filtration column. Fig. 2 shows the elution of the WT and TatAy^{P2A}Cy complexes, with TatCy and TatAy apparent on the Coomassie-stained gels. The levels of TatCy are similar in both cases, but the data again show the presence of much higher levels of TatAy in the elution fractions containing complexes bearing the P2A mutation. Using calibrated size exclusion chromatography we estimated the WT TatAyCy complexes to elute primarily in the range of 350–600 kDa, with a peak of 460 kDa. These sizes are approximate, and are heavily influenced by the detergent micelle. The broad range of elution across a large volume suggests that the WT TatAyCy complex may be rather heterogeneous in size. When the TatAy^{P2A}Cy complexes were run on the same gel filtration column, a large peak was observed in the void volume where complexes greater

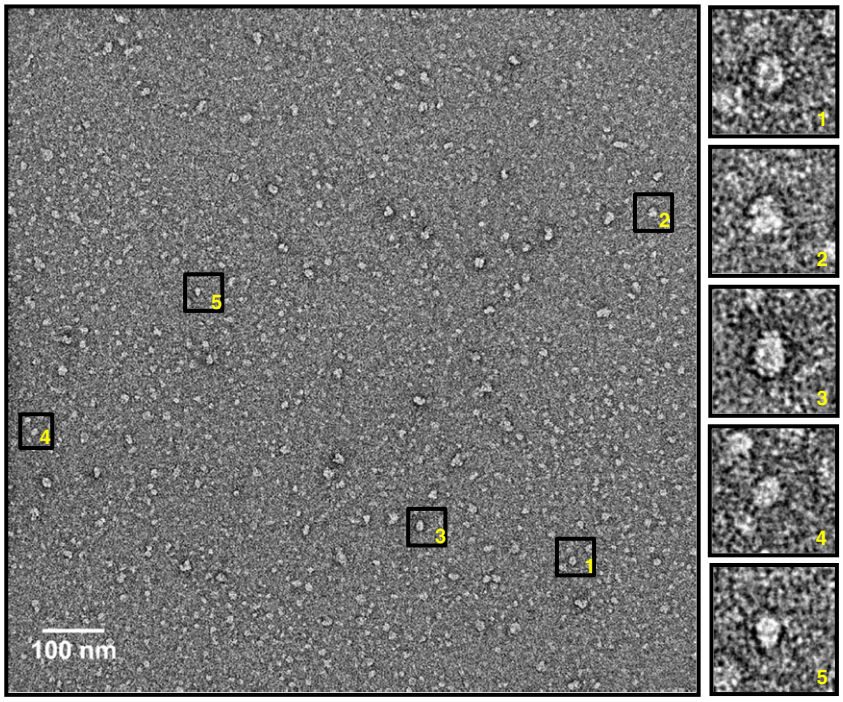

Fig. 3. Electron microscopy of WT TatAyCy complexes shows the presence of discrete particles. The purified WT TatAyCy complexes from gel filtration chromatograhy (fraction 19 in Fig. 2) were negatively stained with uranyl acetate and fixed on a carbon mesh grid. Electron microscopy of WT TatAyCy complexes was performed by Transmission Electron Microscopy at 40,000× magnification (left hand panel). Further magnification of selected TatAyCy complexes is shown in the images on the right.

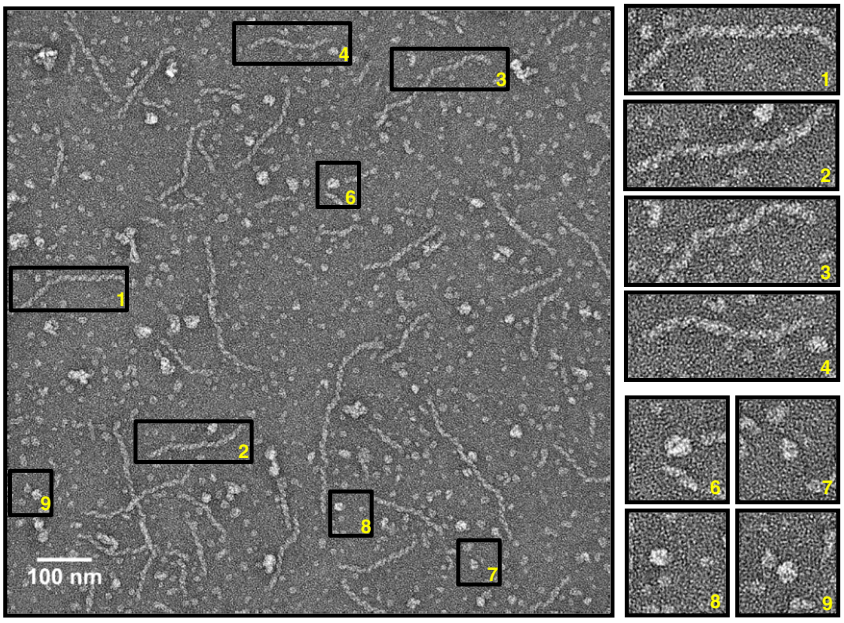

Fig. 4. TatAy^{P2A}Cy complexes form long fibrils. Purified TatAyCy^{P2A} complexes obtained from gel filtration chromatography (fraction 13 in Fig. 2) were negatively stained with uranyl acetate and fixed on a carbon mesh grid. Electron microscopy was performed by Transmission Electron Microscopy at 40,000× magnification (left hand panel). Further magnification of some of the complexes is shown in the images on the right. Some of the complexes are detected as long fibrils whereas others (shown on the right in square boxes) are present as roughly spherical particles.

than 600 kDa are deposited (fractions 12–14 in the elution profile). From this result it can be assumed that a large proportion of the TatAy^{P2A}Cy complexes is ≥600 kDa; these are far larger than the WT complexes.

Analysis of the overall elution profiles shows that some of the TatAy^{P2A}Cy complexes elute in the range of 350–600 kDa, similar to the WT complexes. However, the Coomassie-stained gel shows that these complexes are also abnormal, because they contain much higher levels of TatAy than do the WT complexes. The peak elution fractions for the TatAy^{P2A}Cy complexes contain similar levels of TatCy, but much higher levels of the TatAy protein. Overall, these data indicate that the TatAy^{P2A} assembles with the TatCy subunits with a markedly different stoichiometry, forming complexes that (i) vary dramatically in size, and (ii) contain elevated levels of TatAy. Some of the TatAy^{P2A}Cy complexes elute within the fractionation range of the Superdex 200 column whereas others are too large and elute in the void volume.

3.3. TatAy^{P2A}Cy complexes form long fibrillar structures

It is evident from the purification data that the P2A mutation leads to accumulation of more TatAy with the TatCy-containing complexes. This was considered likely to reflect one of two scenarios: either the TatAyCy complex assembles with an abnormally high number of TatAy^{P2A} subunits, or a more normally-sized TatAy^{P2A}Cy complex associates unusually strongly with separate TatAy^{P2A} complexes. To gain structural insight into the effects of this mutation we employed negative stain electron microscopy as shown in Figs. 3 and 4. Fig. 3 shows data for the WT TatAyCy complex, where samples from the peak gel filtration elution fraction (fraction 19 from Fig. 2, WT) were analysed at 40,000× magnification. Most of the complexes in this fraction appear as particles of between 9 and 16 nm diameters, indicating some heterogeneity in size and form. Some larger irregular complexes of 20–50 nm diameters are also present, and these most likely result from aggregation of the complexes or detergent micelles since they are far too large to elute within the Superdex-200 fractionation range. Further magnification of some of the complexes with a 9–16 nm diameter (right hand images) suggests that they are roughly elliptical with a central cavity/pore-like feature as suggested by density profiling.

Analysis of the TatAy^{P2A}Cy complexes (fraction 13 from Fig. 2, P2A) reveals a very different picture. While some of the complexes have similar overall dimensions to the WT complexes, others form long fibrils of up to 500 nm in length (Fig. 4). Further magnification of the various complexes (right hand panels) shows that the smaller complexes are similar, in overall dimensions, to the WT complexes shown in Fig. 3, although structural differences may not be apparent at this low level of resolution. The fibrillar complexes have a segmented appearance and initial analysis suggests that they are formed from the end-to-end assembly of multiple individual Tat complexes. The images also suggest a spiral organisation (Fig. 5).

We also analysed EM images of additional fractions from the Superdex-200 column, in order to determine the prevalence of fibrils in fractions with differing TatAy^{P2A}:TatCy ratios. The images show that fraction 15 again contains fibrillar complexes, while fraction 17 contains only a few and fraction 22 contains no detectable fibrils. Since the Tat complexes in fractions 17–22 have a TatAy^{P2A}:TatCy ratio that appears similar to that observed with WT complexes in Fig. 2, these data strongly suggest that the fibrillar complexes in fractions 13–15 are built primarily from TatAy^{P2A}. These data thus provide evidence that fibril formation correlates with excess TatAy^{P2A}. The data therefore show that the super-assembly phenotype is caused by the P2A mutation, although an influence of the expression level cannot be excluded since the system is overexpressed in these cells.

3.4. Atomic force microscopy of WT and TatAy^{P2A}Cy complexes

In order to gain additional structural information about the P2A-containing complexes, we studied the WT and the TatAy^{P2A}Cy complexes by AFM, which enables lateral and height measurements of single molecules under liquid and at near-native conditions of temperature, ionic strength and pH. Samples from the elution fractions used for the EM imaging were diluted in AFM imaging buffer then applied to freshly cleaved mica, which provides an atomically flat substrate for adsorbing biomolecules, and imaged by AFM. The AFM topography images of the WT complexes shown in Fig. 6A and B reveal randomly adsorbed individual protein complexes with lateral dimensions (measured as a full width at the half maximum (FWHM)) in the

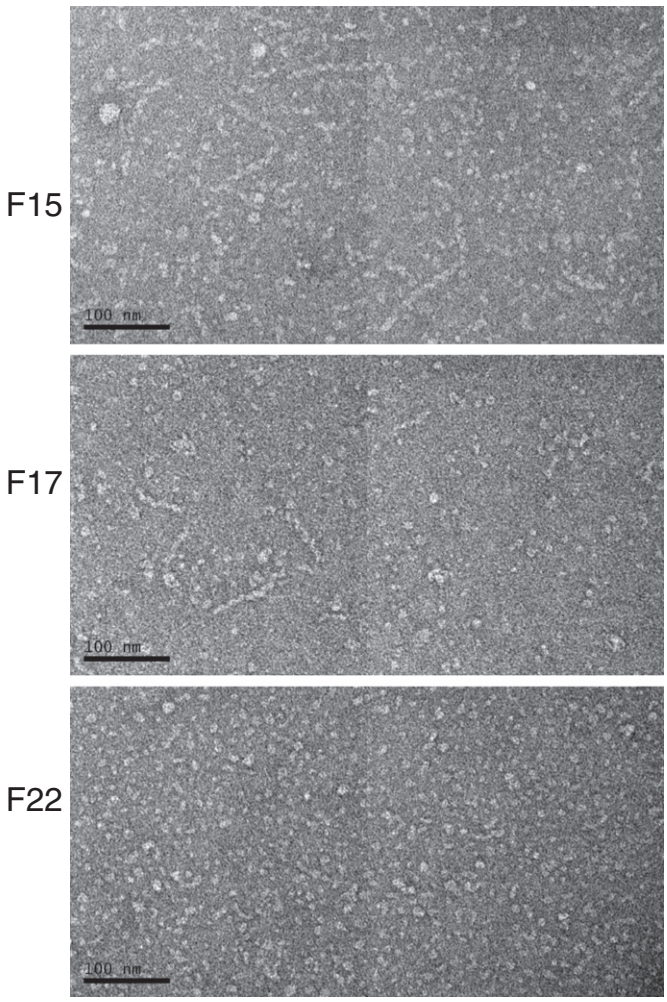

Fig. 5. Fibrillar complexes are found in samples with a high TatAy^{P2A}:TatCy ratio. Purified TatAy^{P2A}Cy complexes obtained from gel filtration chromatography (fractions (F) 15, 17 and 22 in Fig. 2) were negatively stained with uranyl acetate and fixed on a carbon mesh grid. Electron microscopy was performed by Transmission Electron Microscopy at 40,000× magnification.

range 11–15 nm and height in the range 4–5 nm (inset in Fig. 6B) with a small number of larger aggregates (with lateral size and height of up to 35 nm and 15 nm, respectively) present. The data resemble those obtained by EM in Fig. 3. In contrast, the topography images of the TatAy^{P2A}Cy complexes adsorbed on mica (Fig. 6C and D) show a mixture of smaller round features that are similar in size and shape to the WT TatAyCy complexes in Fig. 6A and B, and long fibrils. The contour length of the fibril-like structures was in the range 30–850 nm and their curvature appeared to be random with some relatively sharp bends with radii of curvature down to 10–12 nm. The width of the fibrils measured from the AFM images was in the range 10–15 nm (full width at half maximum; FWHM) and their height was in the range 4–6 nm (see the inset in Fig. 6D). It is worth noting that a slightly wider and higher feature was often found to be attached to at least one of the ends of the fibrils (highlighted with red arrows in Fig. 6D). We hypothesise that these structures may be TatAy^{P2A}Cy complexes, with the remainder of the fibrils formed from recruited TatAy^{P2A} complexes (see below).

Time lapsed AFM imaging also revealed that the fibrils appear to be mobile while adsorbed onto the mica surface at a low enough surface density to provide free spaces around the fibrils. Fig. 6E shows a series of images taken over a 30 min period where significant changes in the conformation of one of the fibrils can be observed. This indicates that the fibrils are weakly adsorbed onto the mica surface, and the most likely cause for the displacement of the fibril is the combination of the thermal excitation from the surrounding medium and the action of the scanning AFM probe (although care was taken to minimise the tip-sample interaction force during imaging as much as possible).

When more concentrated samples of the same TatAy^{P2A}Cy preparation were used for imaging, the fibrils adopted a different conformation (Fig. 7A). In this case the mica surface was covered with closely packed fibrils with very few larger aggregates. Most strikingly, the fibrils were almost perfectly aligned with each other resulting in a very good long range order (see the Fourier transform of the image in the inset in Fig. 7A) with an average lateral period (fibril-to-fibril) of approximately 11.8 nm. While scanning the same area of the sample repeatedly no conformational changes of the fibrils were observed indicating that placing the fibrils at higher density onto the surface greatly reduces their mobility. This helped to achieve better image resolution, which clearly revealed the helical structure of the individual fibrils (Fig 7B). The helical pitch along the individual fibrils varies in the range of 5–11 nm with an average value of 8.3 nm (Fig. 7C). Fig. 7D and E show a false-colour 3-D representation of Fig. 7B, clearly displaying the helical structure of the individual fibrils and the fact that the fibrils adopt the same chirality when adsorbed onto the mica surface.

4. Discussion

Most structural studies on Tat complexes have focused on either the substrate-binding TatC-containing complex or the separate homo-oligomeric TatA-type complex. This is unsurprising since the full, translocation-competent 'super-complex' has proved to be elusive, presumably reflecting its apparently transient nature. In this report we have used a combination of EM and AFM approaches to study a mutated form of the *B. subtilis* TatAy protein in order to acquire structural insights into the Tat complex assembly–disassembly processes. The AFM imaging in particular records high-resolution 3D topographical images of individual fibrils in a native-like environment, that is in buffer solution with physiological pH and ionic strength and without drying, staining, or fixation.

Previous studies on *B. subtilis* Tat complexes have suggested that both the TatAC and TatA-type complexes are present as relatively homogeneous complexes. The TatAdCd complex was shown to run as ca. 230 kDa complexes as judged by Blue-Native polyacrylamide gel electrophoresis and its partner TatAd complex was judged to be ca. 160 kDa using calibrated gel filtration chromatography[8]. A more detailed structural study on the TatAd complex using single particle electron microscopy found that it formed roughly circular complexes of 7.5–9 nm diameters, containing potential cavities or pores of about 3 nm diameter [14]. Other studies on the TatAyCy system showed that both the TatAyCy and TatAy complexes formed ca. 200 kDa complexes [15,18,20,23]. However, as noted above, we have little information on precisely how the TatAC-type and TatA-type complexes interact.

In this study we have analysed a mutated form of TatAy containing a P2A substitution in the short N-terminal extracytoplasmic region. The Tat complexes have been analysed following affinity purification of TatC, which means that our analysis has centred on the TatAyCy complex and any additional complexes that remain associated with this complex during purification. In particular, TatAy complexes would only be pulled down by means of their association with TatAyCy. We show that the P2A substitution has profound effects on complex assembly and dynamics. EM and AFM analyses of the WT TatAyCy complex show the presence of discrete particles that range in diameter from about 9 to 16 nm, in reasonable agreement with the previous studies described above. It is worth noting that whereas AFM provides accurate representations of the true particle height, nonlinear AFM tip convolution effects lead to overestimations of the lateral dimensions of the fibrils. Using the FWHM of the fibril cross-sections takes into account the known AFM tip convolution imaging artefacts and allows a fair

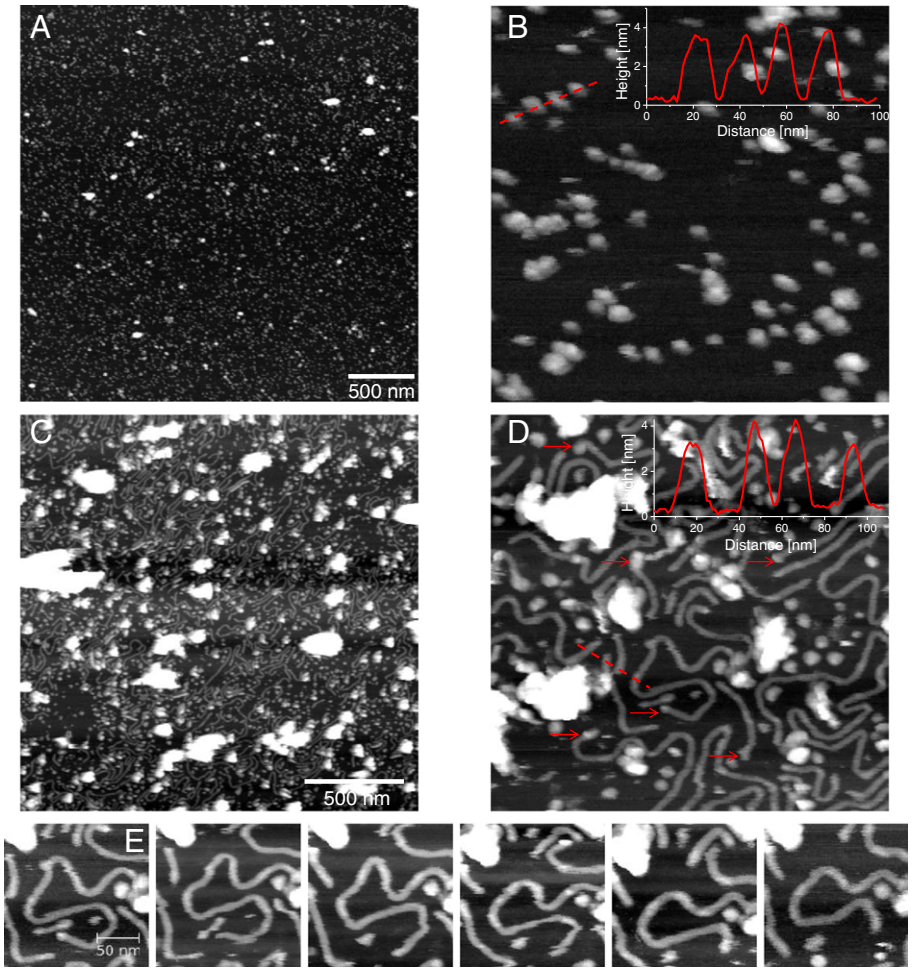

Fig. 6. AFM topography images of WT and TatAy^{P2A}Cy complexes. Both purified WT and TatAy^{P2A}Cy complexes from the gel filtration column were adsorbed onto freshly cleaved mica substrates. The WT complexes (A and B), had lateral dimensions and heights in the ranges 11–15 nm (FWHM) and 4–5 nm, respectively. A cross-section along the dashed line is shown as inset in (B). The TatAy^{P2A}Cy sample (C and D) consisted of a mixture of oval-shaped objects and fibril-like structures with a contour length in the range 30–850 nm and height around 4 nm. The inset in (D) represents a height profile taken across four of the fibrils (dashed line in D). Time-lapsed images (E) of one of the fibrils indicated some mobility even when adsorbed on a mica support. The time interval between the images in (E) is 4.5 min; the Z range (height contrast) of all images is 7 nm.

comparison between AFM and EM data, as shown previously [24]. We also observed that the conventional tapping mode AFM was unsuitable for imaging the fibrils because it disrupted these labile structures; the better force control available in PF-QNM mode was required to obtain topographs of intact fibrils.

In general, bacterial TatC-containing complexes tend to be fairly homogeneous, although the TatAyCy complex does display some heterogeneity as analysed in the present study. However, affinity purification of TatAy^{P2A}Cy complexes revealed the presence of a much larger TatAy:TatCy ratio in the eluate, and the purified complexes were therefore analysed using a combination of biochemical and imaging approaches.

The combined data suggest that the excess TatAy^{P2A} in these preparations cannot be attributed to the assembly of an abnormally high number of TatAy subunits with TatCy in the TatAy^{P2A}Cy complexes. The WT complexes are detected as single particles of 9–16 nm diameters using EM or AFM, and a proportion of TatAy^{P2A}Cy complexes is present as single particles with similar dimensions. Thus, the evidence indicates that the TatAy^{P2A}Cy complexes are relatively similar to WT complexes in terms of overall dimensions. However, a key observation is that the TatAy^{P2A}Cy complexes are part of long (up to 500 nm) fibrils that contain repeating units of particles that resemble the isolated complexes in terms of overall diameter. It is not possible to unambiguously identify repeating units within the fibrils as either TatAy^{P2A}Cy or TatAy^{P2A} complex on the basis of imaging data at this resolution. Nevertheless, the fact that these preparations contain such an abundance of TatAy, relative to TatCy, is good evidence that the majority of the repeating units represent recruited TatAy complexes. We therefore propose that the P2A mutation causes TatAy^{P2A} complexes to hyperassemble with the TatAy^{P2A}Cy complex. It appears likely that fibril formation involves the binding of a TatAy^{P2A} complex to a TatAy^{P2A}Cy complex, after which additional TatAy^{P2A} complexes bind to the growing fibril. If this is the case, it will be interesting to determine whether the overall fibril assembly process involves only a single TatAyCy complex, with the TatAy complexes serially attaching from one direction.

A previous study on the *E. coli* TatABC system likewise showed the presence of long fibrils consisting primarily of TatA [25], and this may point to an inherent ability of TatA-type complexes to self-assemble. However, in that study the *E. coli* TatA-containing fibrils were observed after expression of wild-type TatABC subunits, whereas fibril formation in the present study was strictly associated with the P2A mutation in TatAy. Since wild-type TatAyCy complexes showed no propensity to form fibrils, it is unclear whether the formation of *E. coli* TatA fibrils resulted from the same type of assembly process.

Pro2 is located in the N-terminal extracytoplasmic domain of TatAy, and this domain is extremely short in all TatA/B-family proteins, with the majority of residues localised in the transmembrane span, amphipathic helix or soluble C-terminal domains. However, despite its small size, there are already indications that this region mediates critical protein–protein interactions in TatA/B proteins. A mutagenesis study

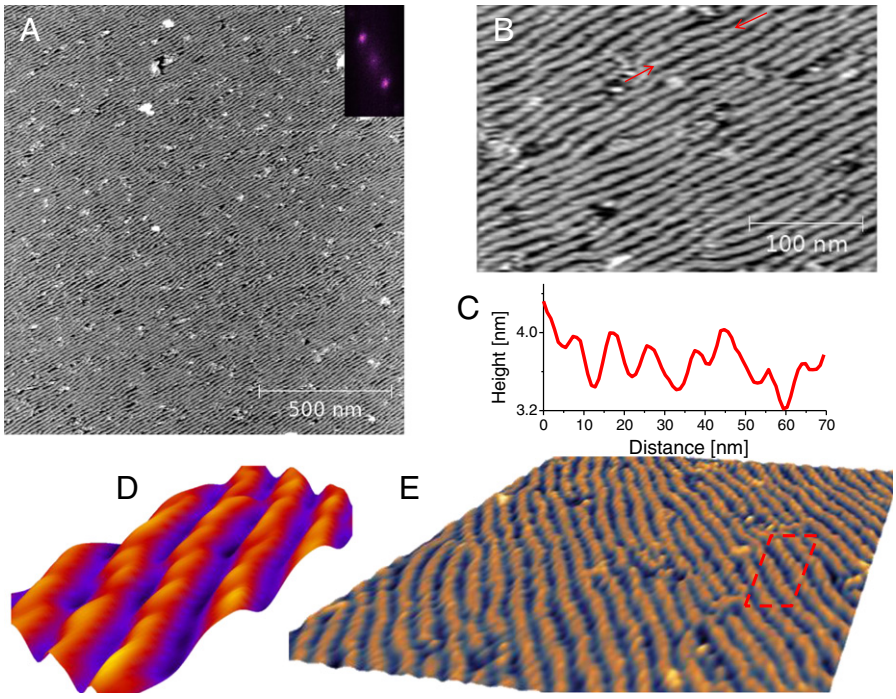

Fig. 7. Helical structure of the TatAy^{P2A}Cy fibrils. AFM topography images of P2A mutant complexes adsorbed at higher concentration (A and B), showing complete coverage of the mica surface and almost perfect long-range order with a fibril-to-fibril distance of 11.8 nm. The helical structure of the fibrils is clearly visible in (B) with a pitch measured along the fibrils in the range 5–11 nm. An example of a line profile taken along the fibril indicated with the arrows in (B) is shown in (C). (E) represents a false-colour 3D rendering of (B) and (D) is a zoom-in within the dashed perimeter in (E). Both 3D images clearly show the helical structure of the fibrils.

on the *E. coli* Tat system revealed that some single-residue substitutions in TatA enabled the protein to rescue a *tatB* null mutant, indicating that the protein could function as TatB within the TatABC complex [26]. These substitutions all mapped to the N-terminal periplasmic domain, indicating that these residues not only mediated key interactions, but also did this in a very TatA- or TatB-specific manner. Similarly, a mutagenesis study on the *B. subtilis* TatAd protein showed that mutations in this region often had severe effects on translocation [10,19]. On the basis of the combined data, we propose that the P2A mutation in TatAy affects the inter-complex interactions with the TatAyCy system and effectively allows an individual TatAy complex to associate more tightly with either TatCy or other TatAy complexes.

Acknowledgements

CGM and JMvD were in parts supported by the CEU projects PITN-GA-2008-215524 (TranSys), LSHG-CT-2006-037469 and 244093, and the transnational SysMO initiative through projects BACELL SysMO1 and 2 with funding from the Research Council for Earth and Life Sciences of the Netherlands Organization for Scientific Research (NWO-ALW). CV and CNH would like to acknowledge the Biotechnology and Biological Sciences Research Council UK (BBSRC) (grant number: BB/G021546/1) for the funding of this work. We are grateful to Ian Hands-Portman for his technical advice and assistance with the electron microscopes and to the Wellcome Trust for generous support (grant ref: 055663/Z/98/Z) to the Imaging Suite at The University of Warwick.

References

[1] J. Fröbel, P. Rose, M. Müller, Twin-arginine-dependent translocation of folded proteins, Philos. Trans. R. Soc. Lond. B Biol. Sci. 367 (2012) 1029–1046.
[2] C. Robinson, C.F.R. Matos, D. Beck, R. Chao, J. Lawrence, N. Vasisht, S. Mendel, Transport and proofreading of proteins by the twin-arginine translocation (Tat) system in bacteria, Biochim. Biophys. Acta 1808 (2011) 876–884.
[3] T. Palmer, B.C. Berks, The twin-arginine translocation (Tat) protein export pathway, Nat. Rev. Microbiol. 10 (2012) 483–496.
[4] C.L. Santini, B. Ize, A. Chanal, M. Müller, G. Giordano, L.F. Wu, A novel sec-independent periplasmic protein translocation pathway in *Escherichia coli*, EMBO J. 17 (1998) 101–102.
[5] J.H. Weiner, P.T. Bilous, G.M. Shaw, S.P. Lubitz, L. Frost, G.H. Thomas, J.A. Cole, R.J. Turner, A novel and ubiquitous system for membrane targeting and secretion of cofactor-containing proteins, Cell 93 (1998) 93–101.
[6] A. Bolhuis, J.E. Mathers, J.D. Thomas, C.M.L. Barrett, C. Robinson, TatB and TatC form a structural and functional unit of the twin-arginine translocase from *Escherichia coli*, J. Biol. Chem. 276 (2001) 20213–20219.
[7] Jan D.H. Jongbloed, U. Grieger, H. Antelmann, M. Hecker, R. Nijland, S. Bron, J.M. van Dijl, Two minimal Tat translocases in *Bacillus*, Mol. Microbiol. 54 (2004) 1319–1325.
[8] J.P. Barnett, R.T. Eijlander, O.P. Kuipers, C. Robinson, A minimal Tat system from a Gram-positive organism: a bifunctional TatA subunit participates in discrete TatAC and TatA complexes, J. Biol. Chem. 283 (2008) 2534–2542.
[9] J.D. Jongbloed, U. Martin, H. Antelmann, M. Hecker, H. Tjalsma, G. Venema, S. Bron, J.M. van Dijl, J. Müller, TatC is a specificity determinant for protein secretion via the twin-arginine translocation pathway, J. Biol. Chem. 275 (2000) 41350–41357.
[10] J.D. Jongbloed, R. van der Ploeg, J.M. van Dijl, Bifunctional TatA subunits in minimal Tat protein translocases, Trends Microbiol. 14 (2006) 2–4.
[11] J.P. Barnett, R. van der Ploeg, R.T. Eijlander, A. Nenninger, S. Mendel, R. Rozeboom, O. P. Kuipers, J.M. van Dijl, C. Robinson, The twin-arginine translocation (Tat) systems from *Bacillus subtilis* display a conserved mode of complex organisation and similar substrate recognition requirements, J. Biol. Chem. 276 (2009) 232–243.
[12] L. Pullan Gohlke, C. McDevitt, I. Porcelli, E. de Leeuw, T. Palmer, H. Saibil, B.C. Berks, The TatA component of the twin-arginine protein transport system forms channel complexes of variable diameter, Proc. Natl. Acad. Sci. U. S. A. 102 (2005) 10482–10486.
[13] J. Baglieri, D. Beck, N. Vasisht, C.J. Smith, C. Robinson, Structure of the TatA paralog, TatE, suggests a structurally homogeneous form of Tat protein translocase that transports folded proteins of differing diameter, J. Biol. Chem. 287 (2012) 7335–7344.
[14] D. Beck, N. Vasisht, J. Baglieri, C.G. Monteferrante, C. Robinson, C.S. Smith, Ultrastructural characterisation of *Bacillus subtilis* TatA complexes suggests they are too small to form homooligomeric translocation pores, Biochim. Biophys. Acta Mol. Cell Res. 1833 (2013) 1811–1819.
[15] M. Alami, I. Luke, S. Deitermann, G.H. Eisner, G. Koch, J. Brunner, M. Müller, Differential interactions between a twin-arginine signal peptide and its translocase in *Escherichia coli*, Mol. Cell 12 (2003) 937–946.
[16] C. Maurer, S. Panahandeh, A.C. Jungkamp, M. Moser, M. Müller, TatB functions as an oligomeric binding site for folded Tat precursor proteins, Mol. Biol. Cell 21 (2010) 4151–4161.
[17] J. Fröbel, P. Rose, F. Lausberg, A.S. Blummel, R. Freudl, M. Müller, Transmembrane insertion of twin-arginine signal peptides is driven by TatC and regulated by TatB, Nat. Commun. 3 (2012) 1311.

[18] S. Zoufaly, J. Fröbel, P. Rose, T. Flecken, C. Maurer, M. Moser, M. Müller, Mapping precursor-binding site on TatC subunit of twin arginine-specific protein translocase by site-specific photo cross-linking, J. Biol. Chem. 287 (2012) 13430–13441.
[19] J.P. Barnett, J. Lawrence, S. Mendel, C. Robinson, Expression of the bifunctional *Bacillus subtilis* TatAd protein in *Escherichia coli* reveals distinct TatA/B-family and TatB-specific domains, Arch. Microbiol. 193 (2011) 583–594.
[20] R. Van der Ploeg, J.P. Barnett, N. Vasisht, C. Robinson, J.-M. van Dijl, Salt-sensitivity of minimal TatAC translocases, J. Biol. Chem. 286 (2011) 43759–43770.
[21] R.S. Bongers, J.W. Veening, M. Van Wieringen, O.P. Kuipers, M. Kleerebezem, Development and characterization of a subtilin-regulated expression system in *Bacillus subtilis*: strict control of gene expression by addition of subtilin, Appl. Environ. Microbiol. 71 (2005) 8818–8824.
[22] J.C. Zweers, T. Wiegert, J.M. van Dijl, Stress-responsive systems set specific limits to the overproduction of membrane proteins in *Bacillus subtilis*, Appl. Environ. Microbiol. 75 (2009) 7356–7364.
[23] J.P. Barnett, R. van der Ploeg, R.T. Eijlander, A. Nenninger, S. Mendel, R. Rozeboom, O.P. Kuipers, J.-M. van Dijl, C. Robinson, The twin-arginine translocation (Tat) systems from *Bacillus subtilis* display a conserved mode of complex organisation and similar substrate recognition requirements, FEBS J. 276 (2009) 232–243.
[24] W. Fritzsche, A. Schaper, T.M. Jovin, Probing chromatin with the scanning force microscope, Chromosoma 103 (1994) 231–236.
[25] F. Berthelmann, D. Mehner, S. Richter, U. Lindenstrauss, H. Lünsdorf, G. Hause, T. Brüser, Recombinant expression of tatABC and tatAC results in the formation of interacting cytoplasmic TatA tubes in *Escherichia coli*, J. Biol. Chem. 283 (2008) 25281–25289.
[26] N. Blaudeck, P. Kreutzenbeck, M. Müller, G.A. Sprenger, R. Freudl, Isolation and characterization of bifunctional *Escherichia coli* TatA mutant proteins that allow efficient tat-dependent protein translocation in the absence of TatB, J. Biol. Chem. 280 (2005) 3426–3432.